Chinese Chemical Letters 35 (2024) 109328

Contents lists available at ScienceDirect

Chinese Chemical Letters

journal homepage: www.elsevier.com/locate/cclet

Nano metal-photosensitizer based on Aza-BODIPY-Cu complex for CDT-enhanced dual phototherapy

Wenjuan Jin, Zelong Chen, Yi Wang, Jiaxuan Li, Jiahui Li, Yuxin Pei, Zhichao Pei*

College of Chemistry & Pharmacy, Northwest A&F University, Yangling 712100, China

ARTICLE INFO

Article history:
Received 28 July 2023
Revised 9 November 2023
Accepted 16 November 2023
Available online 25 November 2023

Keywords:
Nano metal-photosensitizer
Aza-BODIPY-Cu
Coordination self-assembly
Chemodynamic therapy
Dual phototherapy

ABSTRACT

Chemodynamic therapy (CDT) combined with dual phototherapy (photothermal therapy (PTT) and photodynamic therapy (PDT)) is an efficient way to synergistically improve anti-tumor efficacy. However, the combination of multiple modes often makes the composition of the system more complex, which is not conducive to clinical application. In this study, a dual phototherapy ligand carboxyl-modified Aza-BODIPY (BOD-COOH) and metal active center Cu^{2+} were used to construct multiple-modes metal-photosensitizer nanoparticles (BOD-Cu NPs) *via* one-step coordination self-assembly for combination therapy of CDT/PDT/PTT. In order to improve delivery efficiency, the targeted hydrophilic molecule pyridine-modified glucose derivative (G-Py) was synthesized and coated onto the BOD-Cu NPs to form a glycosylated nano metal-photosensitizer BOD-Cu@G by electrostatic interaction. The Cu^{2+} in BOD-Cu@G could not only be used as a coordination node for metal-driven self-assembly but also consume intracellular glutathione (GSH), and then catalyze Fenton-like reaction to generate hydroxyl radical (·OH) for CDT. *In vitro* and *in vivo* studies revealed that BOD-Cu@G could achieve excellent anti-tumor efficiency by CDT-enhanced dual phototherapy.

In anti-tumor therapies, dual phototherapy (PDT combined with PTT) is considered to have high potential in clinical applications due to its advantages in tumor localization, non-invasiveness, and lack of drug-resistance [1,2]. However, hypoxia and overexpressed glutathione (GSH) in the tumor microenvironment limit the anti-tumor efficiency of dual phototherapy [3–5]. Chemodynamic therapy (CDT) is an oxygen-independent reactive oxygen species (ROS) therapy that can generate highly oxidative hydroxyl radicals (·OH) from metal-based materials (such as Cu-, Fe-) by catalyzing Fenton or Fenton-like reaction of hydrogen peroxide (H_2O_2) [6,7]. Meanwhile, some metal-based materials used in CDT can down-regulate GSH *via* redox reaction [8,9]. Therefore, CDT can synergistically improve the anti-tumor efficiency of PDT by consuming GSH and increasing the total amount of ROS in the tumor microenvironment. Furthermore, PTT can promote CDT anti-tumor efficacy by accelerating the reaction rate to increase the generation of ROS [10,11]. Thus, combining CDT with dual phototherapy is an efficient way to synergistically improve anti-tumor efficacy. To date, the nanosystems used in CDT/PDT/PTT mainly consist of inorganic mixed materials [12,13] and inorganic carrier-loaded organic photosensitizer materials [14,15], which have complex compositions and low photosensitizer loading capacities. Hence, the construction of a multiple-mode/functional nanosystem with simple composites and high photosensitizer loading capacity remains a challenge.

Recently, nanoscale metal-organic complex-based phototherapy agents have received increasing attention in tumor treatment due to the advantages of simple preparation, high photosensitizer loading capacity, and multifunction [16–18]. Furthermore, certain metal ions (such as Fe^{2+}, Cu^{2+}, and Mn^{2+}) in metal-organic complex-based phototherapy agents can be used as CDT active centers to combine CDT with PDT [17] or PTT [18]. Regrettably, to date, no nanoscale metal-phototherapy agents have been reported in CDT/PDT/PTT multiple-mode anti-tumor therapy. We have therefore set out to construct a one-step coordinatively self-assembled nano metal-photosensitizer with a simple composition based on metal ion and dual-photosensitizer [19–21] that possesses both photodynamic and photothermal activity through one wavelength light source excitation, which can achieve CDT/PDT/PTT combination therapy.

Aza-BODIPY is a newly discovered fluorescent dye molecule with a high molar extinction coefficient and excellent photostability. Recent studies demonstrated that Aza-BODIPY exhibits both photothermal and photodynamic activity under excitation of one specific wavelength of near-infrared (NIR) light [22,23], and can

* Corresponding author.
E-mail address: peizc@nwafu.edu.cn (Z. Pei).

https://doi.org/10.1016/j.cclet.2023.109328
1001-8417/

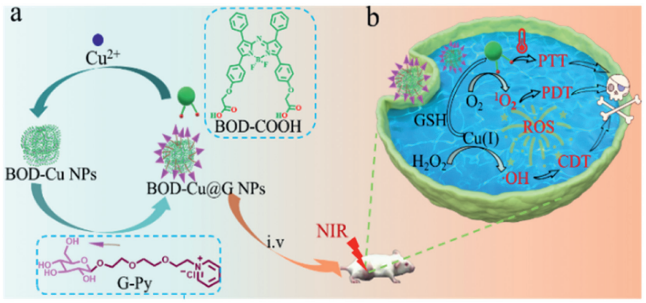

Scheme 1. (a) The construction of BOD-Cu@G NPs. (b) The synergistic effects of PTT/PDT/CDT in tumor treatment.

be easily structurally modified [24]. These advantages make it attractive as a dual phototherapy ligand in the construction of nano metal-photosensitizers.

Herein, we report for the first time the construction of a nanoscale glycosylated metal-photosensitizer (BOD-Cu@G) based on carboxyl group modified Aza-BODIPY (BOD-COOH) and Cu^{2+} (coordination node and CDT active center) coordinatively self-assembling into the nano complex BOD-Cu NPs. The targeted hydrophilic small molecule pyridine-modified glucose derivative (G-Py) was coated onto BOD-Cu NPs to improve biocompatibility and targetability by electrostatic interaction (Scheme 1a). BOD-Cu@G could accumulate in tumor cells by Warburg effect [25], then consume GSH and generate ·OH for CDT. At the same time, dual-photosensitizer BOD-COOH could generate singlet oxygen ($^1O_2$) and localized high temperature by 685 nm light irradiation. The localized high temperature could also promote the CDT reaction, further improving the total ROS production to achieve CDT-enhanced dual phototherapy anti-tumor efficiency (Scheme 1b). This glycosylated nano metal-photosensitizer can not only achieve the combination of CDT/PDT/PTT but also has the characteristics of simple composition, high photosensitizer loading capacity, and targeted delivery.

The synthesis details of carboxyl-modified Aza-BODIPY (BOD-COOH) [26,27] are described in Figs. S1 and S2 (Supporting information). The BOD-Cu NPs were prepared by a simple hydrothermal method [28], and the DLS analysis shows (Fig. S11a in Supporting information) that the average diameter of BOD-Cu NPs is 293 nm, the polydispersity index (PDI) is 0.206 and the zeta potential is −25.3 mV. As shown in Fig. 1a, the UV–vis characteristic absorption peak of BOD-Cu (728 nm) has a significant red shift ($\Delta = 68$ nm) compared to BOD-COOH (660 nm). Similarly, as depicted in the IR spectra (Fig. 1d), the stretching vibration of –C=O (1739 cm^{-1}) in BOD-COOH shifts to a lower wavenumber (1600 cm^{-1}) in BOD-Cu and BOD-Cu@G NPs. To further clarify the coordination state of copper ions, XPS was used to analyze the valence state of copper ions in BOD-Cu NPs. As shown in Figs. 1e and f, the characteristics binding energies of Cu^{2+} are 954.7 eV and 934.8 eV, corresponding to Cu $2p_{1/2}$ and Cu $2p_{3/2}$ respectively, while the obvious satellite peaks between the two peaks indicated that the copper is Cu^{2+} in BOD-Cu NPs. The composition of BOD-Cu NPs was also confirmed by ICP-MS, with the ratio of Cu^{2+} to BOD-COOH in BOD-Cu NPs being 2.7 by calculation.

Due to the negative charge of BOD-Cu NPs, the positively charged G-Py (the synthesis details are described in Figs. S3–S10 in Supporting information) [29] could coat their surfaces to form the BOD-Cu@G NPs through electrostatic interactions, which increases the zeta potential of BOD-Cu@G NPs significantly from −25.3 mV to −20.2 mV. G-Py could also effectively improve the hydrophilicity and tumor targeting of BOD-Cu@G NPs due to the excellent biocompatibility of glucose and the Warburg effect of tumor cells [25]. DLS analysis showed that the average diameter of BOD-Cu@G is 302 nm, the PDI is 0.282 (Fig. 1g), and it has good stability in water (Fig. S11b in Supporting information) as well as 10% FBS-containing PBS solution (Fig. S11c in Supporting information). The shape of BOD-Cu@G NPs was characterized by SEM (Fig. 1h) and TEM (Fig. 1i). Moreover, the absorption (Fig. 1b) and fluorescence spectra (Fig. 1c) of BOD-Cu@G NPs in the presence of GSH (10 mmol/L) were consistent with BOD-COOH, which proved that the Cu^{2+} in BOD-Cu@G NPs could consume GSH by redox reaction and then release BOD-COOH.

The photothermal ability of BOD-Cu@G NPs and BOD-COOH was investigated under 685 nm light irradiation (Fig. 2a). The results showed that the temperature increase of BOD-Cu@G NPs aqueous solution has a concentration (Fig. 2b) and light power (Fig. S12a in Supporting information) dependence. The temperature increase ($\Delta T = 26.4$ °C) and photothermal conversion efficiency η [30] of BOD-Cu@G NPs ($\eta = 57.1\%$) were much higher than BOD-COOH ($\Delta T = 22.6$ °C, $\eta = 31.4\%$) (Fig. S12b in Supporting information), which proved that BOD-Cu@G NPs have excellent photothermal conversion capability. As shown in Fig. 2c, the photothermal curve from five cycles was very stable and did not attenuate, which proved that BOD-Cu@G NPs have excellent photothermal stability.

DPBF is a fluorescent probe that reacts with certain ROS, such as $^1O_2$ and ·OH, and can therefore be used to measure the amount of ROS generated [31]. As shown in Fig. 2d, the BOD-Cu@G group could generate limited ·OH in the presence of GSH (10 mmol/L) and H_2O_2 (0.1 mmol/L). In contrast, the most efficient reduction by the BOD-Cu@G group was observed when irradiation with 685 nm light occurred with the presence of GSH and H_2O_2.

ESR spectroscopy was used to further prove the generation of ·OH and $^1O_2$ by BOD-Cu@G. DMPO was used as the ·OH radical scavenger, and TEMP was used as the $^1O_2$. radical scavenger [32,33]. As shown in Fig. 2e, a 1:2:2:1 characteristic ESR signal of ·OH was observed in the BOD-Cu@G group with GSH and H_2O_2. As expected, under light irradiation (685 nm, 160 mW/cm^2, 2 min), the photothermal effect increased the formation of ·OH. Under light irradiation of 685 nm (160 mW/cm^2) for 2 min without GSH and H_2O_2, an obvious 1:1:1 characteristic ESR signal of $^1O_2$ was observed in the BOD-COOH and BOD-Cu@G groups. Therefore, BOD-Cu@G can produce two free radicals (·OH, and $^1O_2$) simultaneously under light irradiation in the presence of GSH and H_2O_2.

The generation of ROS in A549 cells was evaluated by DCFH-DA [34]. As shown in Fig. 3a, without light irradiation, compared to the obvious green fluorescence of the BOD-Cu@G group, the green fluorescence of the BOD-COOH group was very weak, which indicates that BOD-Cu@G could generate ROS (·OH) by Fenton-like reaction, while BOD-COOH could not. In contrast, under 685 nm light irradiation, both BOD-COOH and BOD-Cu@G groups display obvious green fluorescence (Fig. 3b), but the fluorescence intensity of BOD-Cu@G group remained significantly higher.

The extracellular and intracellular GSH consumption were measured by Micro reduced glutathione assay kit. As shown in Fig. S13a (Supporting information), the relative extracellular GSH concentration did not change in the BOD-COOH group but decreased by 42% in the BOD-Cu@G group (50 μg/mL). Furthermore, after treatment with BOD-Cu@G for 6 h, compared to the PBS group, the relative intracellular GSH concentration decreased by 22% (Fig. S13b in Supporting information). These results demonstrate that the Cu^{2+} in the BOD-Cu@G NPs can consume GSH and reduce its capture of ROS [35].

Glucose transporters (GLUTs) are proven to be overexpressed on the cell membranes of cancer cells [36,37]. The cellular uptake of BOD-Cu@G by tumor cells (A549) and normal hepatocytes (HL7702) was investigated using CLSM (Fig. 4a). Compared with the faint red fluorescence of BOD-Cu@G in HL7702 cells, A549 cells showed strong red fluorescence, indicating an increased uptake

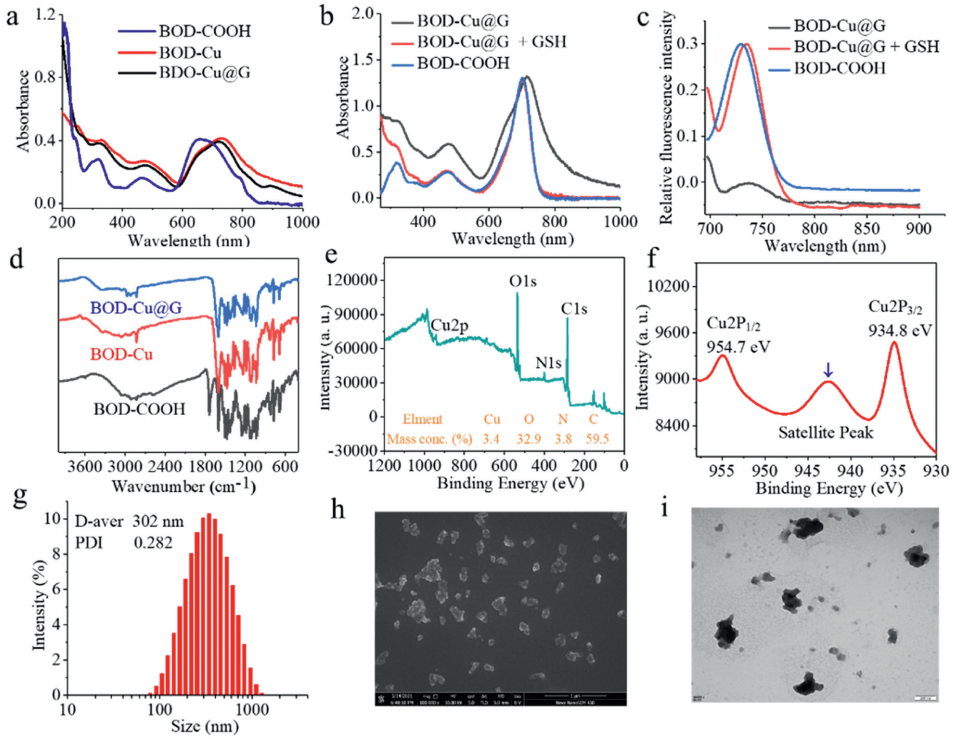

Fig. 1. Characterization of BOD-Cu@G NPs. (a) UV–vis spectra of BOD-COOH, BOD-Cu NPs, and BOD-Cu@G NPs in water. (b) UV–vis spectra and (c) fluorescence spectrum of BOD-COOH, BOD-Cu@G NPs, and BOD-Cu@G NPs + GSH (10 mmol/L) in DMSO (*Ex*/*Em*: 692/725 nm). (d) IR spectra of BOD-COOH, BOD-Cu NPs, and BOD-Cu@G NPs. (e) XPS analysis of BOD-Cu NPs. (f) The local enlarged drawing of (e) is in the range of 930–960 eV. (g) DLS analysis of BOD-Cu@G NPs aqueous solution. (h) SEM image of BOD-Cu@G NPs. Scale bar: 1 μm. (i) TEM image of BOD-Cu@G NPs. Scale bar: 200 nm.

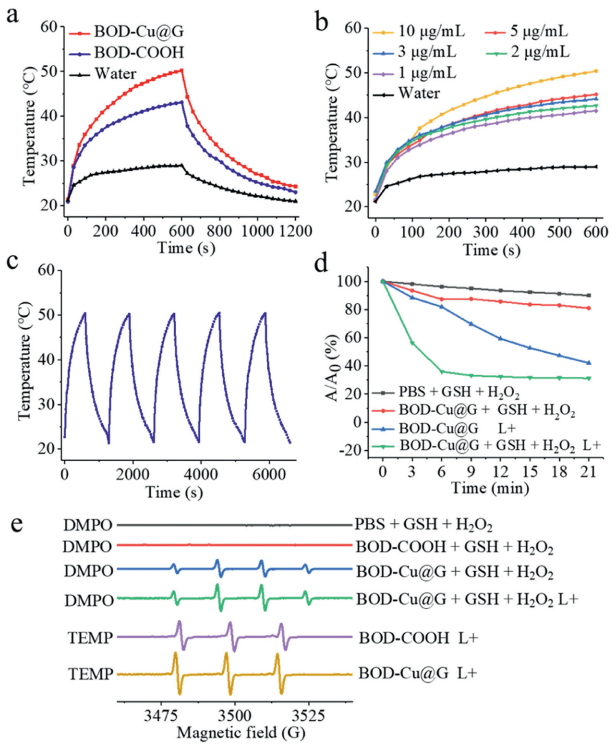

Fig. 2. (a) Photothermal curves of different solutions under 685 nm light irradiation (160 mW/cm^2). (b) Photothermal heating curves of BOD-Cu@G NPs aqueous solutions with different concentrations under 685 nm light irradiation (160 mW/cm^2) for 10 min. (c) Photothermal stability test of BOD-Cu@G NPs aqueous solutions (10 μg/mL) under 685 nm light irradiation of 160 mW/cm^2. (d) ROS generation of BOD-Cu@G NPs. (e) ESR spectra of different reaction systems for the BOD-COOH and BOD-Cu@G (L+ means 685 nm light irradiation of 80 mW/cm^2).

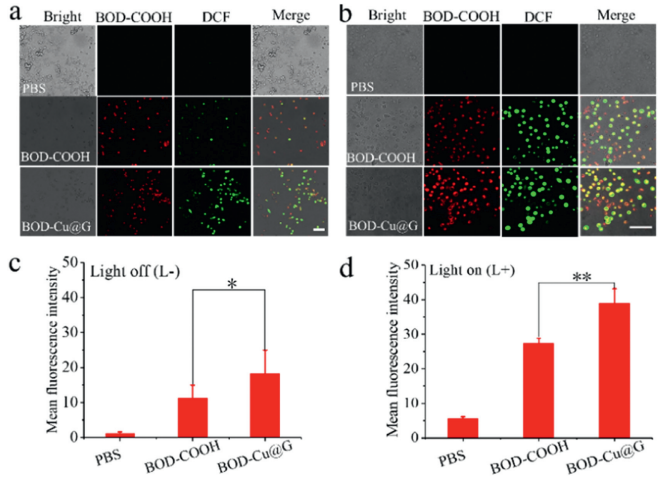

Fig. 3. (a) Confocal laser scanning microscopy (CLSM) images of A549 cells incubated with PBS, BOD-COOH, and BOD-Cu@G respectively for 6 h. (b) CLSM images of A549 cells incubated with PBS, BOD-COOH, and BOD-Cu@G respectively for 6 h followed by light irradiation at 685 nm, 80 mW/cm^2 for 20 min. (c) and (d) Mean fluorescence intensity of DCF for (a) and (b). The concentration of BOD-Cu@G and BOD-COOH were 5 μg/mL respectively. Scale bar: 100 μm. E_x/E_m: 637/730 nm for BOD-COOH and BOD-Cu@G; E_x/E_m: 488/530 nm for DCF. ($n = 5$, $^{***}P < 0.001$, $^{**}P < 0.01$, or $^{*}P < 0.05$).

due to their higher number of GLUTs. To further prove this conclusion, glucose was used to pre-treat A549 cells. The fluorescence intensity observed in pre-treated A549 cells was clearly weaker than untreated A549 cells (Fig. 4c). The results were further confirmed with flow cytometry (FCM) in Fig. 4b. In addition, the cellular uptake of BOD-Cu@G was found to be time-dependent. CLSM analysis of A549 cells incubated with BOD-Cu@G demonstrated increase

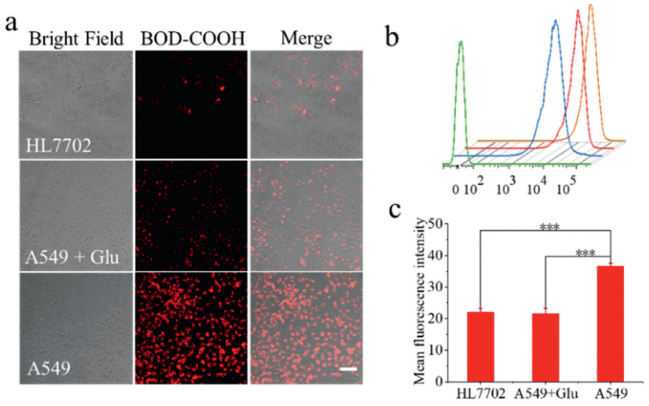

Fig. 4. Targeting ability of BOD-Cu@G was detected by CLSM (a) (scale bar: 200 μm. E_x/E_m: 637/730 nm for BOD-COOH) and FCM (b) (control (green), HL7702 (blue), A549 + Glu (red), A549 (orange)). (c) Mean fluorescence intensity of (a). The concentration of BOD-Cu@G was 5 μg/mL, the incubation time was 6 h. $n = 3$, $^{***}P < 0.001$, $^{**}P < 0.01$, or $^{*}P < 0.05$.

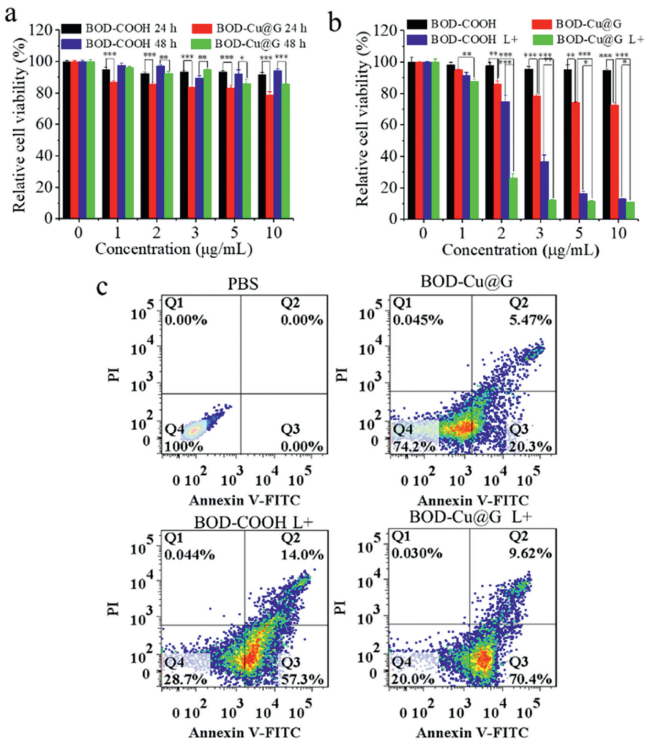

Fig. 5. (a) Cell viability of HL7702 cells. (b) Cell viability of A549 cells. ($n = 5$, $^{***}P < 0.001$, $^{**}P < 0.01$, or $^{*}P < 0.05$). (c) Annexin V-FITC/PI apoptosis assay of A549 cells with different treatments. The concentration was 5 μg/mL respectively. Light condition: 685 nm light irradiation of 80 mW/cm^2 for 20 min.

in red fluorescence with amount of incubation time (Fig. S14a in Supporting information). The result was further corroborated with FCM (Fig. S14b in Supporting information). The same result was observed in Hela, MCF-7, and HepG2 tumor cells incubated with BOD-Cu@G NPs (Fig. S15 in Supporting information). The above experiments proved that the internalization pathway of BOD-Cu@G NPs is glucose-mediated endocytosis, which specifically improves the uptake of BOD-Cu@G by tumor cells.

The cytotoxicity (dark toxicity and phototoxicity) of BOD-Cu@G NPs and BOD-COOH against HL7702 cells (Fig. 5a) and A549 cells (Fig. 5b) were assessed using an MTT assay. Under dark condition, the viability of HL7702 cells incubated with BOD-Cu@G NPs was 85.6%, which was slightly lower than BOD-COOH treated cells (93.9%). The viability of A549 cells incubated with BOD-Cu@G NPs was 72.7% compared to 94.8% in the BOD-COOH group. The moderate dark toxicity of BOD-Cu@G NPs to A459 cells may be caused by ·OH of CDT. In terms of phototoxicity, the viability of A549 cells incubated with BOD-Cu@G NPs was notably reduced compared to those treated with BOD-COOH after light irradiation (685 nm, 80 mW/cm^2 for 20 min). As further evidence, Annexin V-FITC/PI apoptosis assay was conducted to determine the extent of cell death under various conditions. Apoptosis and necrosis of A549 cells treated with BOD-Cu@G NPs + light irradiation (80.0%) was much higher than the dual phototherapy group (BOD-COOH + light irradiation, 71.3%) and CDT group (BOD-Cu@G without light irradiation, 25.8%) (Fig. 5c).

The cytotoxicity and phototoxicity of BOD-Cu@G NPs to other tumor cells (HeLa, MCF-7, and HepG2) were also studied by MTT assay, yielding similar results to A549 cells (Fig. S16 in Supporting information). Under light irradiation, when the concentration was greater than 5 μg/mL, the cell inhibition rate of BOD-COOH and BOD-Cu@G are similar. But at lower concentrations (2–3 μg/mL), the cell inhibition rate of BOD-Cu@G was significantly higher than BOD-COOH. Without light irradiation, the cell inhibition rate of BOD-Cu@G in concentrations of 1–10 μg/mL were higher than the equivalent concentrations of BOD-COOH. The preceding experimental results reaffirm the CDT activity of BOD-Cu@G in the absence of light irradiation, while also demonstrating its ability to combine CDT with dual phototherapy, facilitated by light irradiation, to further enhance anticancer efficacy.

In order to evaluate the *in vivo* safety of BOD-Cu@G, the blood of healthy BALB/c mice with different concentrations of BOD-Cu@G was collected at 24 h after injection for hematological analysis. As shown in Fig. S17, the blood indices of healthy BALB/c mice injected with BOD-Cu@G had no significant difference with the control group. These results indicate that BOD-Cu@G has no acute toxicity under treatment dose. Next, IR thermal camera was used to record *in vivo* thermal IR images from H22 tumor-bearing mice injected with BOD-Cu@G NPs after 0, 12, 24, 36, and 48 h, respectively. The tumor temperature was highest after 24 h, at 47.1 °C (Fig. S18 in Supporting information). To compare the *in vivo* efficacy of BOD-Cu@G, thermal IR images of BOD-Cu@G NPs, BOD-COOH, and PBS treated mice (24 h after intravenous injection) were captured (Fig. 6a). The temperature of BOD-COOH and BOD-Cu@G NPs group increased to 44.0 °C and 47.1 °C, respectively, within 3 min while the PBS-injected mouse showed only a ~4 °C increase to 36.8 °C under the same irradiation. The above data also indicate that BOD-Cu@G NPs strongly aggregate at the tumor site.

The *in vivo* tumor inhibition experimental scheme is shown in Fig. 6b. The weight of tumor-bearing mice in all groups did not significantly change within 20 days (Fig. 6d). In contrast, the tumor sizes of PBS, BOD-COOH, and BOD-Cu@G groups increased rapidly during 20 days, but the tumor sizes and weight of BOD-COOH L+ and BOD-Cu@G L+ groups were significantly suppressed (Fig. 6c and f). Importantly, compared to the BOD-COOH L+ group, the tumor of the BOD-Cu@G L+ group was completely inhibited (without recurrence). As shown in Fig. 6g, compared with the dual phototherapy group BOD-COOH L+ and the CDT group (BOD-Cu@G), BOD-Cu@G with light irradiation induced clear tumor tissue damage and necrosis/apoptosis through enhanced phototherapy effect of CDT/PDT/PTT combination. In contrast, the BOD-COOH group caused negligible injury to the tumor tissue. The tissue sections of the major organs of both groups had no noticeable histopathological lesions (Fig. S19 in Supporting information).

In summary, a glycosylated nano metal-photosensitizer BOD-Cu@G was constructed for CDT/PDT/PTT combination therapy by hydrophilic molecule pyridine-modified glucose derivative and nano metal-photosensitizer (BOD-Cu NPs) that coordinatively self-assemble from a dual-photosensitizer (BOD-COOH) and a CDT ac-

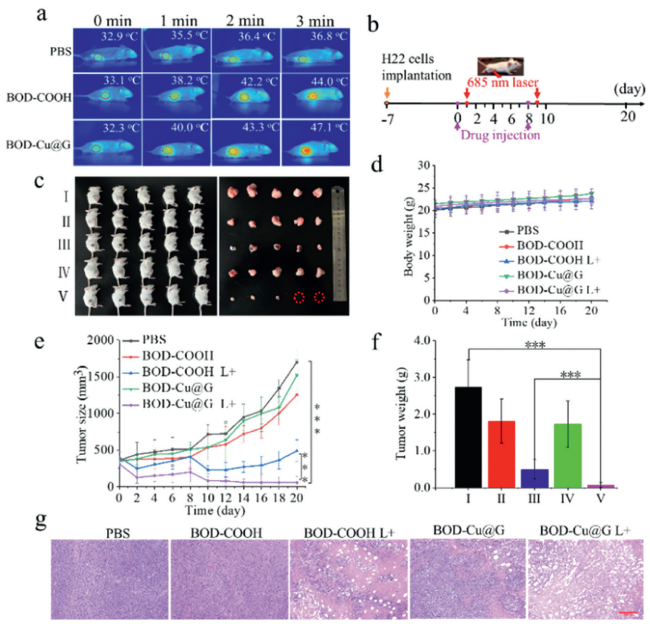

Fig. 6. (a) Thermal IR images of H22 tumor-bearing mice. (b) Schematic diagram of the treatment process. (c) Photographic images of H22 tumor-bearing BALB/c mice and excised tumors and (f) tumor weight (I: PBS, II: BOD-COOH, III: BOD-COOH L+, IV: BOD-Cu@G, V: BOD-Cu@G L+) at the 20th-day post-injection. (d) Body weight change of mice. (e) Change in tumor volumes. (g) H&E staining images of tumor tissue. Scale bar: 200 μm. L+ means 685 nm laser at 2 W/cm^2 for 3 min, $n = 5$, $^{*}P < 0.05$, $^{**}P < 0.01$, $^{***}P < 0.001$.

tive center (Cu^{2+}). CLSM and FCM proved that BOD-Cu@G can target the tumor cells by the Warburg effect. XPS analysis showed that the copper in the BOD-Cu nano complex was Cu^{2+}, which can consume GSH and catalyze Fenton reaction to generate ·OH. The photothermal conversion efficiency of BOD-Cu@G NPs is 57.1%, and the generation of ROS (·OH and $^1O_2$) was demonstrated by DPBF consumption and ESR analysis. BOD-Cu@G NPs with irradiation show a strong inhibitory effect through CDT-enhanced dual-phototherapy on a variety of tumor cells (A549, HeLa, HepG2, and MCF-7). *In vivo* anti-tumor evaluation also demonstrated that BOD-Cu@G has a significantly enhanced phototherapy effect compared to BOD-COOH under irradiation. This glycosylated nano metal-photosensitizer system provides a novel platform for CDT-enhanced dual phototherapy, which has broad application potential in anti-tumor treatments.

Declaration of competing interest

The authors declare that they have no known competing financial interests or personal relationships that could have appeared to influence the work reported in this paper.

Acknowledgments

This work was supported by the National Natural Science Foundation of China (No. 22171230) and the Project of Science and Technology of Social Development in Shaanxi Province (No. 2023-YBSF-151). The authors thank Life Science Research Core Services (LSRCS), Northwest A&F University for helping with characterizations including SEM, TEM, CLSM, HRMS, and flow cytometry.

Supplementary materials

Supplementary material associated with this article can be found, in the online version, at doi:10.1016/j.cclet.2023.109328.

References

[1] J. Chen, Y. Cui, K. Song, et al., Biomater. Sci. 9 (2021) 2115–2123.
[2] J.P. Wei, X.L. Chen, X.Y. Wang, et al., Chin. Chem. Lett. 28 (2017) 1290–1299.
[3] Y. Jin, Y. Guo, J. Yang, et al., Adv. Mater. 35 (2023) 2209690.
[4] J. Yuan, R. Peng, D. Su, et al., Theranostics 11 (2021) 3502–3511.
[5] M. Zuo, W. Qian, M. Hao, et al., Chin. Chem. Lett. 32 (2021) 1381–1384.
[6] Z. Tang, Y. Liu, M. He, et al., Angew. Chem. Int. Ed. 58 (2019) 946–956.
[7] K. Yang, S. Qi, X. Yu, et al., Angew. Chem. Int. Ed. 61 (2022) e202203786.
[8] J. Dong, Y. Yu, Y. Pei, et al., J. Colloid Interface Sci. 607 (2022) 1651–1660.
[9] J. Li, H. Tian, F. Zhu, et al., Adv. Healthc. Mater. 11 (2022) 2201986.
[10] Y. Shi, J. Zhang, H. Huang, et al., Adv. Healthc. Mater. 9 (2020) 2000005.
[11] B. Zou, Z. Xiong, L. He, et al., Biomaterials 285 (2022) 121549.
[12] Y. Liang, C. Liao, X. Guo, et al., Small 19 (2023) 2205511.
[13] H. Zhang, R. Han, P. Song, et al., J. Colloid Interface. Sci. 629 (2023) 103–113.
[14] L. Sun, J. Wang, J. Liu, et al., Small Struct. 2 (2021) 2000112.
[15] Y. Jiang, Y. Lu, L. Lei, et al., Mater. Sci. Eng. C 130 (2021) 112465.
[16] B. Li, X. Wang, L. Chen, et al., Theranostics 8 (2018) 4086–4096.
[17] H.S. Jung, S. Koo, M. Won, et al., Chem. Sci. 14 (2023) 1808–1819.
[18] X. Li, D. Xi, M. Yang, et al., Adv. Healthc. Mater. 10 (2021) 2101008.
[19] Y. Tang, L. Xue, Q. Yu, et al., ACS Appl. Bio Mater. 2 (2019) 5888–5897.
[20] B. Zhu, F. Qu, D. Bi, et al., ACS Appl. Mater. Interfaces 15 (2023) 9135–9149.
[21] G. Wan, Y. Cheng, J. Song, et al., Chem. Eng. J. 380 (2020) 122458.
[22] W. Feng, Y. Lv, Z. Chen, et al., Chem. Eng. J. 417 (2021) 129178.
[23] W. Jin, Z. Chen, S. Yang, et al., Chem. Commun. 58 (2022) 12584.
[24] Y. Qu, W. Jin, Y. Wan, et al., Chin. Chem. Lett. 35 (2024) 108493.
[25] B.I. Reinfeld, M.Z. Madden, M.M. Wolf, et al., Nature 593 (2021) 282–288.
[26] D. Wu, H.C. Daly, E. Conroy, et al., Eur. J. Med. Chem. 161 (2019) 343–353.
[27] L. Shi, F. Hu, Y. Duan, et al., ACS Nano 14 (2020) 2183–2190.
[28] Y. Wan, Z. Chen, Y. Wang, et al., Carbohydr. Polym. 311 (2023) 120762.
[29] Y. Wang, Y. Wen, Y. Qu, et al., J. Colloid Interface Sci. 615 (2022) 386–394.
[30] J. Cao, J. Chi, J. Xia, et al., ACS Appl. Mater. Interfaces 11 (2019) 25720–25729.
[31] Z. Shi, X. Meng, K. Zhang, et al., ACS Mater. Lett. 3 (2021) 781–789.
[32] Q. Li, J. Yu, L. Lin, et al., ACS Appl. Mater. Interfaces 15 (2023) 16482–16491.
[33] Y. Shen, Y. Sun, R. Yan, et al., Biomaterials 148 (2017) 31–40.
[34] M. Yang, S. Cao, X. Sun, et al., Bioconjug. Chem. 31 (2020) 663–672.
[35] P. An, F. Fan, D. Gu, et al., J. Control. Release 321 (2020) 734–743.
[36] S. Liu, Z. Sun, M. Liang, et al., Adv. Sci. 9 (2022) 2105315.
[37] P. Ma, G. Wei, J. Chen, et al., Drug Deliv. 28 (2021) 2256–2267.